

Achieving optimal rectification using underdamped rocked ratchets

Fabio Marchesoni,^{1,2} Sergey Savel'ev,^{1,3} and Franco Nori^{1,4}

¹Frontier Research System, The Institute of Physical and Chemical Research (RIKEN), Wako-shi, Saitama, 351-0198, Japan

²Dipartimento di Fisica, Università di Camerino, I-62032 Camerino, Italy

³Department of Physics, Loughborough University, Loughborough LE11 3TU, United Kingdom

⁴Center for Theoretical Physics, Department of Physics, University of Michigan, Ann Arbor, Michigan 48109-1040, USA

(Received 23 June 2005; revised manuscript received 13 October 2005; published 10 February 2006)

An underdamped rocked ratchet operated at very low temperatures and damping is shown: (i) to be capable of rectifying the ac input signal more efficiently than in the overdamped regime; (ii) to be insensitive to the initial conditions, at variance with noiseless, or deterministic, ratchets; and (iii) to be characterized by a wide damping “window,” where its efficiency is appreciable also for weak input amplitudes. All these properties are rather robust, irrespective of the wave form of the drive and the ratchet potential. Our results relate to recent experiments on current-biased annular Josephson junctions and also on rectifiers of magnetic flux quanta in superconductors.

DOI: 10.1103/PhysRevE.73.021102

PACS number(s): 05.40.-a, 05.60.Cd, 74.50.+r

I. INTRODUCTION

Particles in an asymmetric device can drift, on average, in one direction even when the time and space averages of all applied macroscopic forces or gradients are zero. To achieve directed transport in such a device, called a ratchet, a time-correlated source of energy is required, for instance, non-Markovian external fluctuations (thermal ratchets [1]) or a drive periodic in time (rocked ratchets [2]); under more general conditions, directed motion can be induced also by non-equilibrium white-noise sources [3]. In signal analysis notation, a ratchet can be regarded as a signal rectifier. Rocked ratchets transporting massive particles exhibit strong inertial effects capable of reversing their current [4]. Moreover, inertial rocked ratchets naturally develop a chaotic dynamics, when thermal fluctuations are switched off (deterministic or noiseless ratchets) [5–7].

A deterministic ratchet may be mapped to an asymmetric damped-driven pendulum [8–10]. The phase-space portrait of a regular damped-driven pendulum was computed by Hieberman *et al.* [8], who revealed the existence of delocalized, symmetric strange attractors with an intricate structure on all scales, later recognized to be fractal objects [10]. Its running orbits can be either periodic or diffusive, depending on the value of an appropriate control parameter (e.g., the potential amplitude); their average direction is determined by the pendulum initial conditions.

Not surprisingly, *noiseless* ratchets operated in the underdamped regime are extremely sensitive to the initial conditions [6]. For sufficiently massive particles, the coexistence of regular trajectories with a periodicity that is a multiple of the driving cycle, makes the ratchet characteristics largely unpredictable (both in magnitude and sign); on further increasing the mass of the particle, all trajectories become fully diffusive and the ratchet current drops to zero [7].

In this paper we show that adding a certain amount of noise, no matter how small, changes this pattern dramatically. We investigate the transport of particles of unit mass for very low-temperature ratchets driven by a periodic force $F(t)$ with angular frequency Ω much lower than the fre-

quency ω_0 of a particle oscillating at the bottom of a potential well (adiabatic regime). The damping constant γ is varied from exceedingly large values $\gamma \sim 10\omega_0$, where the overdamped (Smoluchowski) approximation adopted in the earlier ratchet literature [1] holds well, deep into the underdamped regime $\gamma \sim 10^{-3}\omega_0$. The main findings of our analysis are as follows. (i) The rectification power of the ratchet increases with decreasing γ and is the largest in an optimal damping window (γ_m, γ_M), independently of the ac drive amplitude. (ii) Under the adiabatic conditions $\Omega \ll \gamma_m, \omega_0$, no current inversions occur within the optimal rectification window; the ratchet current is insensitive to the initial conditions also in the zero-temperature limit $T \rightarrow 0$ (i.e., for $T=0+$), at variance with the corresponding noiseless (or $T=0$) case addressed in the previous literature [6,7].

Results (i) and (ii) are of potential application in the design and operation of high-performance, dependable rectifiers, such as arrays of Josephson junctions [11], long Josephson junctions [12], asymmetric superconducting quantum interference device (SQUIDs) [13,14], and bona fide quantum electronic devices [15]. For example, in an asymmetric SQUID [13,14] the damping constant $\gamma \propto 1/RC$ can be easily changed by varying the device temperature T , as the resistance R grows fast with T . Thus, an asymmetric SQUID seems to be a very promising candidate to observe the predicted crossover between the overdamped and underdamped rectification regimes.

II. NUMERICAL RESULTS

We simulated the archetypal model of a damped rocked ratchet [2], namely, a unit mass Brownian particle obeying the Langevin equation [16]

$$\ddot{x} = -\gamma\dot{x} - V'(x) + \xi(t) + F(t), \quad (1)$$

where (i) the random force $\xi(t)$ is a stationary Gaussian noise of vanishing mean, $\langle \xi(t) \rangle = 0$, and autocorrelation function

$$\langle \xi(t) \xi(0) \rangle = 2 \gamma k T \delta(t), \quad (2)$$

modeling an equilibrium heat bath; (ii) the viscous constant γ quantifies the damping (or inertial) effects; and (iii) the applied drive $F(t)$ is periodic in time. To avoid harmonic mixing effects [17,18], we chose simple wave forms, such as a sinusoidal signal,

$$F(t) = A \cos(\Omega t), \quad (3)$$

or an up-down periodic ramp,

$$F(t) = A \left(1 - \frac{4|t|}{T_\Omega} \right) \quad (4)$$

with $|t| \leq T_\Omega/2$ and $T_\Omega = 2\pi/\Omega$. In both cases, the time origin can be changed arbitrarily. (iv) The potential $V(x)$ describes the particle glide substrate; it is periodic with period L , namely, $V(x+L) = V(x)$, and asymmetric under reflection, $V(x+x_0) \neq V(-x+x_0)$ for any $x_0 \in [0, L]$.

We have simulated two types of ratchet potentials, (i) the *harmonic* potential

$$V_h(x) = -\frac{L}{2\pi} \left[\sin\left(\frac{2\pi x}{L}\right) + \frac{1}{4} \sin\left(\frac{4\pi x}{L}\right) \right] \quad (5)$$

with $L=1$. Each potential unit cell is characterized by a fundamental frequency at the well bottom, $\omega_0 \approx 3.18$, and a peak-to-peak amplitude $\Delta V \approx 0.35$; the static depinning thresholds of the tilted potential $V(x) \mp |F|x$, are $F_{3R}=3/4$, to the right (-), and $F_{3L}=3/2$, to the left (+). (ii) The *piecewise linear* potential

$$V_l(x) = -Q \left(\frac{x}{L_2} + \frac{1}{2} \right) \quad -L_2 < x < 0, \\ = Q \left(\frac{x}{L_1} - \frac{1}{2} \right) \quad 0 < x < L_1, \quad (6)$$

with $L_1+L_2=L$ and $L=1$. Here, the barrier height ΔV coincides with Q and the depinning forces to the right and to the left are $F_{3R}=Q/L_1$ and $F_{3L}=Q/L_2$, respectively; to ensure the same ratchet polarity as in Eq. (5), we took $L_1 > L_2$. Moreover, as the frequency of the particle oscillations at the well bottoms are amplitude dependent, we choose $\omega_0 = \sqrt{Q/L_2}$ for convenience.

On numerically integrating the stochastic differential equation (1), we computed the time-averaged particle velocity $\langle \dot{x} \rangle \equiv v$ as a function of the damping constant γ for different drive amplitudes A . We present here only two data sets: Fig. 1 for the harmonic potential $V_h(x)$ and Fig. 2 for the piecewise linear potential $V_l(x)$, both driven by the double-sided ramp force (4). For the sake of comparison to the analytical predictions shown in Sec. III, v is expressed in units of A/γ , the expected maximum drift velocity of the driven particle. Moreover, both figures are composed of three panels, respectively, for $A > F_{3L}$, $F_{3R} < A < F_{3L}$, and $A < F_{3R}$ (i.e., for A larger, between, and smaller than the right and/or left depinning thresholds of the relevant potential). All curves on display refer to thermal energies kT not larger than 20% of the potential barrier ΔV .

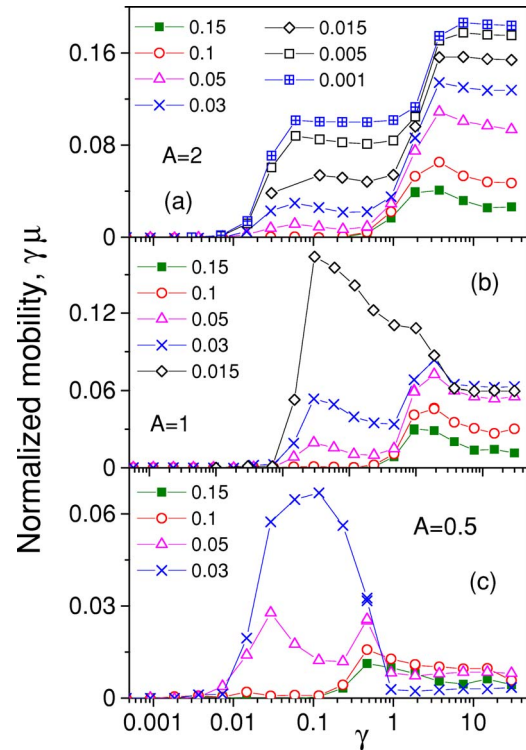


FIG. 1. (Color online) Response function, $\gamma v/A \equiv \gamma \mu$ vs damping γ , of the inertial ratchet (1) with drive (4) and harmonic potential (5) for (a) $A=2$, (b) $A=1$, (c) $A=0.5$, and different values of kT . Other simulation parameters are $L=1$ and $\Omega=10^{-3}$.

A few remarkable properties are apparent by inspection: (i) The curves v versus γ exhibit a simple and stable structure. The net velocity v increases with lowering γ faster than the scaling law γ^{-1} predicted in the overdamped regime [1]; the rectification effect appears to be very strong in a well-defined damping window (γ_m, γ_M) with $\gamma_m \approx 10^{-2} \omega_0$ and $\gamma_M \approx \omega_0$, independently of the drive amplitude.

(ii) For our choice of the simulation parameters, no current inversions have been detected. Note that $v=0$ for $\gamma < \gamma_m$, so that Ω turns out to be the slowest effective frequency and/or rate of the process (i.e., $\Omega \ll \gamma, \omega_0$); as a consequence, all our data can be analyzed within an adiabatic approximation scheme. Current inversions do occur for higher forcing frequencies [4].

(iii) An accurate sampling of the particle phase space led us to conclude that the curves v versus γ (in Fig. 1) are insensitive to the initial conditions $[x(0), \dot{x}(0)]$. At variance with the literature on deterministic ratchets [5–7], the response of a zero-temperature ratchet is a truly stationary observable. Of course, the relevant transient times grow exponentially long for $kT/\Delta V$ tending to zero—and so do our simulation runs.

The boundaries γ_m and γ_M of the optimal rectification interval are insensitive both to the drive frequency (not shown), at least in the adiabatic regime $\Omega \rightarrow 0$, and to the noise intensity, as long as $kT \ll \Delta V$. This suggests that γ_m and γ_M are quantities only determined by the substrate potential.

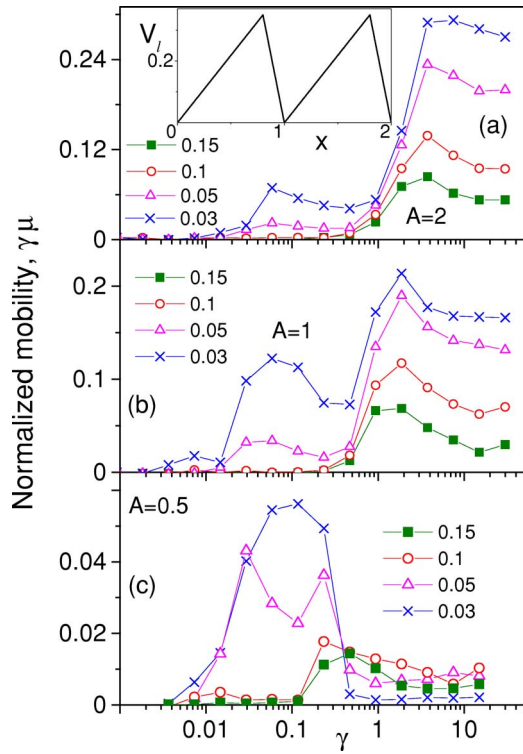


FIG. 2. (Color online) Response function, $\gamma v/A \equiv \gamma\mu$ vs damping γ , of the inertial ratchet (1) with drive (4) and piecewise linear potential (6) for (a) $A=2$, (b) $A=1$, (c) $A=0.5$, and different values of kT . Other simulation parameters: $Q=0.35$, $L_1=0.8$, $L_2=0.2$, and $\Omega=10^{-3}$. The potential profile is drawn in the inset of panel (a).

III. ANALYTICAL TOOLS

To interpret the simulation data reported in Sec. II, one needs to generalize the theory of the underdamped Brownian motion in a symmetric washboard potential (Sec. III A), developed by Risken [16] and co-workers, to the case of the asymmetric ratchet potentials studied here (Sec. III B).

A. Mobility: Zero-noise versus zero-temperature limit

Let us first consider Eq. (1) for a static dc drive F pointing in a fixed direction, say to the right, $F>0$. As shown in Ref. [16], the corresponding particle dynamics is characterized by random switches between a locked state with zero average velocity and a running state with asymptotic average velocity $v=F/\gamma$. In terms of the particle mobility, $\mu=v/F$, locked and running states correspond to $\gamma\mu=0$ and $\gamma\mu=1$, respectively.

In the overdamped regime of Eq. (1), the particle sits at a local minimum of the tilted substrate as long as F is smaller than the relevant depinning threshold, denoted here by F_3 ; for $F>F_3$, there exist no such minima and the particle runs in the F direction with average speed approaching F/γ .

In the underdamped regime $\gamma \ll \omega_0$, the locked-to-running transition depends crucially on the presence of noise, no matter how weak. In the *noiseless* case, $T=0$, the average speed of a Brownian particle depends on the initial conditions according to the hysteretic cycle illustrated in Fig. 3(a). The transition from the locked to the running state occurs on

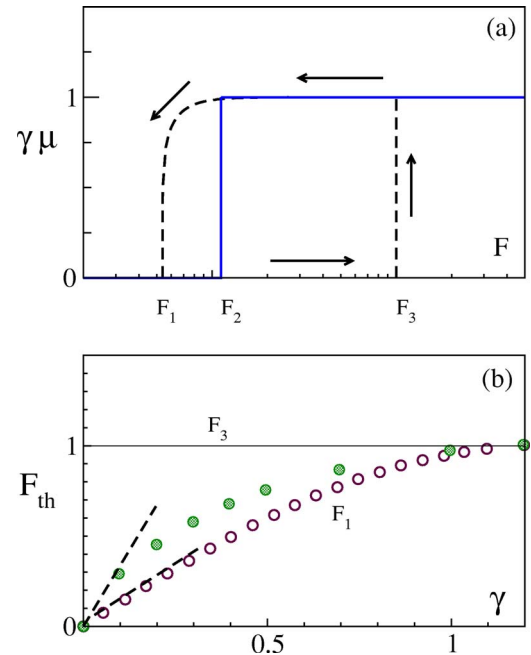


FIG. 3. (Color online) Underdamped particle ($\gamma=0.03$) in the symmetric washboard potential $V(x)=\omega_0^2 \cos x$ with $\omega_0=1$ and $L=2\pi$. (a) The locked-to-running states transition. The thresholds $F_1=(4/\pi)\omega_0\gamma$ (pinning) and $F_3=\omega_0^2$ (depinning) of the hysteretic loop (dashed curves) and the zero-temperature step at $F_2=3.36\omega_0\gamma$ (solid curve) are marked explicitly; (b) the locked-to-running transition threshold F_{th} at $kT=0.3$ is plotted vs γ (solid circles); simulation data bridge the zero-temperature asymptotes F_2 ($\gamma \rightarrow 0$, dashed tangent line) and F_3 ($\gamma \rightarrow \infty$, solid line) [19]. Simulation data (empty circles) for F_1 vs γ are plotted for a comparison; the dashed tangent line at the origin represents the analytical approximation $F_1=(4/\pi)\omega_0\gamma$ for $\gamma \rightarrow 0$.

raising F above F_3 (depinning threshold), while the opposite transition takes place on lowering F below a certain repinning threshold $F_1=\kappa_1\gamma\omega_0$. For sufficiently large values of γ , in the damped regime with $\gamma \approx \omega_0$, F_1 approaches F_3 , and the hysteretic cycle collapses into a single transition step.

For vanishingly low temperatures, $T=0+$, the scenario changes completely, as the underdamped *stationary* dynamics of $x(t)$ is controlled by only one threshold $F_2=\kappa_2\gamma\omega_0$: For $F < F_2$, the Brownian particle remains trapped in one potential well; for $F > F_2$, it falls down the tilted washboard potential with average speed close to F/γ . At the transition threshold F_2 , the quantity $\gamma\mu$ jumps from zero to (very close to) one, stepwise [Fig. 3(a)].

At variance with F_3 , the threshold F_2 indicates a dynamical transition that occurs for quite small static tilts. For practical purposes, resolving F_2 requires relatively long observation times [16,20] because, at threshold, the dynamics of the particle is energetically bistable and the locked-to-running switches take an exponentially long Kramers' time to occur, namely, an average time proportional to $e^{\delta V/kT}$. As a consequence, ramping F up and down over an appropriate interval to determine F_2 (either numerically or experimentally) is a critical procedure [19]. Ramping periods any shorter than the characteristic locked-to-running switching times cause hysteretic loops of the particle velocity, and the width of such

loops in the vicinity of the threshold gets markedly enhanced on lowering the temperature [19]; hence, the need for exceedingly long observation times in the limit $T \rightarrow 0$.

Therefore, at finite but very low temperatures, i.e., as long as $kT \ll \Delta V$, an appropriate locked-to-running transition threshold F_{th} is numerically identifiable with high accuracy at any value of γ ; as displayed in Fig. 3(b), on increasing γ , F_{th} as a function of γ bridges monotonically the two asymptotes $F_{\text{th}}(\gamma \rightarrow 0) = F_2$ and $F_{\text{th}}(\gamma = \infty) = F_3$ discussed in this section.

B. Asymmetric thresholds

The ratchet response for $F > 0$ (particle drifting to the right) and $F < 0$ (particle drifting to the left) is different. This amounts to introducing two distinct mobility functions, respectively, $\mu_R(F) \equiv \mu(F)$ and $\mu_L(F) \equiv \mu(-F)$; the quantities $\mu_R(F)$ and $\mu_L(F)$ are both non-negative definite for $F \geq 0$ and, due to the ratchet asymmetry, $\mu_R(F) \neq \mu_L(F)$. This means that we have to determine two sets of thresholds F_{1R} , F_{2R} , and F_{3R} for $\mu_R(F)$ and F_{1L} , F_{2L} , and F_{3L} for $\mu_L(F)$.

The depinning thresholds of the potentials used in our simulations have been reported in Sec. II, i.e., (i) harmonic potential (5), $F_{3R} = 3/4$, $F_{3L} = 3/2$; (ii) piecewise linear potential (6), $F_{3R} = Q/L_1$, $F_{3L} = Q/L_2$.

The determination of the repinning thresholds is less trivial. In order to skip tedious algebraic passages, we refer the reader directly to Eq. (11.190) of Ref. [16]. For $\gamma \rightarrow 0$, a simple energy balance argument yields

$$\frac{F_{1R}}{\gamma} = \frac{F_{1L}}{\gamma} = \bar{v}(\Delta V), \quad (7)$$

where $\bar{v}(E) = \int_0^L \sqrt{2[E - V(x)]}/L$. This integral can be calculated analytically for the piecewise linear potential $V_l(x)$, i.e., for $\gamma \rightarrow 0$,

$$F_{1R} = F_{1L} = \frac{2}{3} \gamma \sqrt{2\Delta V} \quad (8)$$

with $\Delta V = Q$. Equation (8), with the appropriate ΔV , provides a working estimate for the pinning thresholds of the harmonic potential $V_h(x)$, too, as proven by numerical computation. In conclusion, for $\gamma \rightarrow 0$

$$F_{1R} = F_{1L} = \kappa_1 \omega_0 \gamma \quad (9)$$

with $\kappa_1 \approx 1.06$ for $V_h(x)$ and $\kappa_1 = 2\sqrt{2L_2}/3$ for $V_l(x)$. Note that higher-order (γ/ω_0)-corrections to Eq. (7) are sensitive to the potential asymmetry, so that $F_{1R} \neq F_{1L}$.

Locating the zero-temperature transition thresholds is far more complicated. Following Risken's prescription (see Sec. 11.6.3 of Ref. [16]), one obtains an implicit integral equation for F_{2R} and F_{2L} in the $\gamma \rightarrow 0$ limit. As such an equation is symmetric under the transformation $V(x) \rightarrow -V(x)$, one concludes that $F_{2R} = F_{2L} = F_2$, where

$$\int_0^{(F_2/\gamma)} dx \int_0^x \frac{dy}{\bar{v}(y)} = \Delta V \quad (10)$$

and \bar{v} is the function introduced in Eq. (7). From the numerical integration of Eq. (10), we obtain the limiting expressions for the $T=0+$ transition thresholds

$$F_{2R} = F_{2L} = \kappa_2 \omega_0 \gamma \quad \text{for } \gamma \rightarrow 0. \quad (11)$$

Here, $\kappa_2 \approx 3.5$ for $V_h(x)$ and $\kappa_2 \approx 2.5\sqrt{L_2}$ for $V_l(x)$; note that κ_2 and κ_1 are of the same order of magnitude with $\kappa_2 > \kappa_1$ [20].

Finally, when plotted versus γ , the zero-temperature transition thresholds for F pointing both right, $F_{\text{th},R}$, and left, $F_{\text{th},L}$, start out tangent to $F = \kappa_2 \omega_0 \gamma$ at $\gamma = 0$, and then bend toward their horizontal asymptotes, F_{3R} and F_{3L} , for $\gamma \in (\gamma_m, \gamma_M)$. The thresholds $F_{\text{th},R}$ and $F_{\text{th},L}$ versus γ can be extracted from our simulation data for both potential $V_l(x)$ and $V_h(x)$; the two curves never cross at finite γ , i.e., $F_{\text{th},L} > F_{\text{th},R}$ for $\gamma > 0$. Note that the analytical determination of F_{th} as a function of γ is impossible even in the symmetric case of Fig. 3(b) [16]. However, explicit numerical calculations indicate that $F_{1R}(\gamma)$ and $F_{1L}(\gamma)$ merge with F_{3R} and F_{3L} , respectively, for γ of the order of ω_0 ; hence, the estimate $\gamma_M \approx \omega_0$ [16]. The γ dependence of the corrections to the approximate identity $F_{\text{th},R} \approx F_{\text{th},L}$ for $\gamma \ll \gamma_m$ is quite hard to handle. Here, we limit ourselves to remark that the dimensionless ratio γ/ω_0 depends neither on Ω/ω_0 nor on $kT/\Delta V$, as we are considering the adiabatic limit, $\Omega \rightarrow 0$, of the ratchet response at zero temperature, $T=0+$. It follows that γ_m is also a ratchet constant proportional to ω_0 .

C. Zero-temperature ratchet current

An analytical estimate of the particle time-averaged current in the piecewise linear potential (6) is affordable without much effort both at $T=0+$ and $T=0$.

In the zero-temperature limit, the transition thresholds $F_{\text{th},R}$ and $F_{\text{th},L}$ are well defined. As shown in Sec. III A, we can assume that $\mu(F_{\text{th},-}) = 0$ and $\mu(F_{\text{th},+}) = 1$ with high accuracy, both for the right and left mobility curves. For simplicity, we report here our results for the periodic double-sided ramp (4), valid under adiabatic conditions $\Omega \ll \gamma, \omega_0$, namely,

$$v(A) = \frac{A^2 - F_{\text{th},R}^2}{4\gamma A}, \quad F_{\text{th},R} < A < F_{\text{th},L} \quad (12a)$$

$$= \frac{F_{\text{th},L}^2 - F_{\text{th},R}^2}{4\gamma A}, \quad A > F_{\text{th},L}, \quad (12b)$$

and $v(A) = 0$ for $A < F_{\text{th},R}$. A plot of the curve $v(A)$ is displayed in Fig. 4(a). The rising branch (12a) only occurs when the particle may depin to the right (i.e., for $F_{\text{th},R} < A < F_{\text{th},L}$); depinning in both directions for $A > F_{\text{th},L}$ degrades the rectification effect, as indicated by the decaying tail (12b) of $v(A)$. Note that for $\gamma \rightarrow \infty$, $F_{\text{th},R}$ and $F_{\text{th},L}$ approach the γ -independent limits, F_{3R} and F_{3L} , respectively; hence, $v(A) \propto \gamma^{-1}$, as expected [1]. On the contrary, the peak of the rectification current, $v(F_{\text{th},L})$, in the underdamped regime $\gamma \ll \omega_0$ is γ independent; however, note that for $\gamma \rightarrow 0$ the two thresholds tend to coincide (i.e., $F_{\text{th},R} \rightarrow F_{\text{th},L}$). The last remark has a bearing on our interpretation of the simulation data of Sec. II.

The noiseless case, $T=0$, is briefly addressed here for the sake of a comparison to the zero-temperature case. Let us assume that the hysteretic cycle in Fig. 3(a) can be approxi-

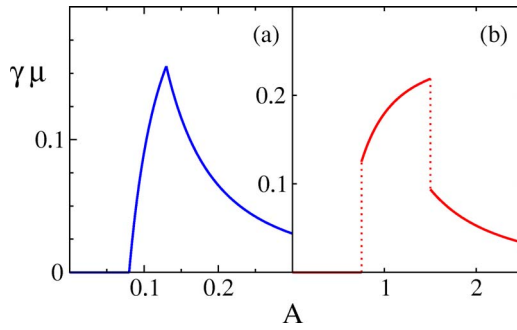


FIG. 4. (Color online) Underdamped particle ($\gamma=0.03$) in the asymmetric potential (5) with $L=2\pi$: Mobility curves $\mu(A)$ for (a) $T=0+$, Eq. (12), and (b) $T=0$, Eq. (13). Note that the rectification curve in (b) matches recent experimental data in Ref. [24].

mated to a rectangle with $\gamma\mu_R=0$ for F increasing from F_{1R} up to F_{3R} , and $\gamma\mu_R=1$ for F decreasing from F_{3R} down to F_{1R} . Let us also impose the same approximation for the left mobility μ_L by replacing the suffix R with L . The resulting trajectories can be either regular (with the period equal to an integer multiple of the forcing cycle T_Ω) or chaotic, depending on the initial conditions. Optimal rectification is obtained for periodic trajectories with period T_Ω ; in the adiabatic limit, the maximum rectification current induced by the drive (4) on the ratchet potential $V_l(x)$ is [7]

$$v(A) = \frac{A}{4\gamma} - \frac{F_{3R}^2 - F_{1R}^2}{8\gamma A}, \quad F_{3R} < A < F_{3L} \quad (13a)$$

$$= \frac{(F_{3L}^2 - F_{3R}^2) - (F_{1L}^2 - F_{1R}^2)}{8\gamma A}, \quad A > F_{3L}, \quad (13b)$$

and $v(A)=0$ for $A < F_{3R}$. This curve [shown in Fig. 4(b)] exhibits two jumps at $A=F_{3R}$, from $v(F_{3R}-)=0$ to $v(F_{3R}+)= (F_{3R}^2 - F_{1R}^2)/(8\gamma F_{3R})$, and at $A=F_{3L}$, from $v(F_{3L}-)=v_0 + F_{3L}^2/(8\gamma)$ down to $v(F_{3L}+)=v_0 - F_{1L}^2/(8\gamma F_{3L})$, with $v_0 = (F_{3L}^2 - F_{3R}^2 + F_{1R}^2)/(8\gamma F_{3L})$. Such discontinuities are peculiar to the response curve of any underdamped ratchet device in the $T=0$ (or deterministic) regime [7,12], irrespective of the actual potential profile and driving wave form. Note that here the current peak $v(F_{3L}-)$ for $\gamma \rightarrow 0$ shoots up like γ^{-1} , at variance with $v(F_{th,L})$ from Eq. (12).

IV. DATA INTERPRETATION

In Sec. III, we have outlined the theoretical framework needed to interpret the simulation results reported in Sec. II. To make contact with our analytic predictions, we remind the reader that our numerical data have been plotted in units of A/γ [i.e., must be compared to $\gamma\mu(A) \equiv \gamma v(A)/A$].

Figures 1 and 2 are both made of three panels for decreasing values of the drive amplitude, namely, $A > F_{3L}$ in panels (a), $F_{3R} < A < F_{3L}$ in panels (b), and $A < F_{3R}$ in panels (c). The three panels show, besides an apparent difference for large γ , suggestive similarities. Most notably, the γ dependence of the net ratchet current at low temperature can be

separated into three well-distinguishable domains delimited by γ_m and γ_M . More specifically, for:

(i) $\gamma < \gamma_m$: The reason why the current drops sharply to zero for $\gamma \leq \gamma_m$ is clear from Fig. 3(b). No matter what the value of A , as γ tends to zero, A ends up being larger than both thresholds $F_{th,R}$ and $F_{th,L}$; thus, from Eq. (12b) we conclude that the relevant quantity $\gamma\mu \approx (F_{th,L}^2 - F_{th,R}^2)/(4A^2)$ vanishes, since the two thresholds merge into one another (i.e., $F_{th,L} \rightarrow F_{th,R}$, for $\gamma \rightarrow 0$).

(ii) $\gamma > \gamma_M$: The zero-temperature transition thresholds are insensitive to γ for $\gamma > \gamma_M \sim \omega_0$. This simplifies the analysis of our simulation data. In view of Eq. (12), $\gamma\mu$ is predicted to be independent of γ for $A > F_{3R}$, see Figs. 4(a) and 4(b), and drop to zero for $A < F_{3R}$, see Fig. 4(c);

(iii) $\gamma_m < \gamma < \gamma_M$: On decreasing γ below ω_0 the right and the left zero-temperature thresholds start departing from their asymptotic values F_{3R} and F_{3L} . This produces different behaviors as γ grows smaller than ω_0 , depending on the value of A . For $A > F_{3L}$, the gap between A and the larger threshold $F_{th,L}$ widens; correspondingly, the net velocity (12b) starts decaying monotonically to zero. For an intermediate-to-small drive amplitude, $A < F_{3L}$, the curve $\gamma\mu = (A^2 - F_{th,R}^2)/(4A^2)$ bends upward—note that $F_{th,R}$ decreases monotonically with decreasing γ . Moreover, since $F_{th,L}$ is also a decreasing function of γ , on lowering γ , $F_{th,L}$ eventually crosses A ; as a consequence, $\gamma\mu$ reaches a plateau and then bends downward, as explained in item (i).

We stress the fact that inertial ratchets operated in the optimal damping window (γ_m, γ_M) are also capable of rectifying efficiently weak-amplitude input signals with $A < F_{3R}$. On regarding γ_m as the damping value where the curves $F_{th,L}(\gamma)$ and $F_{th,R}(\gamma)$ part from the common asymptote $F_2(\gamma)$, then an underdamped ratchet at low temperature can be sensitive to sinusoidal signals with amplitude as small as $F_2(\gamma_m)$. Note that such an effect is *enhanced* by lowering the temperature to zero, whereas overdamped ratchets can rectify subthreshold ac signals only if assisted by noise [2].

The temperature dependence of the curves v versus A is also worth discussing. The analytical approach of Sec. III does not apply for small but finite $kT/\Delta V$. As shown in Fig. 11.27 of Ref. [16], on increasing T the sharpness of the mobility steps of Fig. 3(a) decreases; therefore, the rectification efficiency of the ratchet diminishes substantially away from the right and/or left thresholds. As a result, $\gamma\mu$ develops broad bumps for γ values corresponding to $F_{th,L}$ crossing A for $F_{3R} < A < F_{3L}$, and either $F_{th,R}$ or $F_{th,L}$ crossing A for $A < F_{3R}$. A similar effect was detected in the current dispersion of an underdamped rocked ratchet (see Fig. 1 of Ref. [21]).

The temperature dependence of $\gamma\mu$ is displayed in Fig. 5. In the overdamped region $\gamma > \gamma_M$ [panel (b)], for $A < F_{3R}$, the ratchet velocity goes through a maximum for an optimal value of T , as known from the previous literature in Smoluchowski's (or zero-mass) approximation [2]; for $A > F_{3R}$, the ratchet performs better in the $T=0+$ limit (i.e., its efficiency gets degraded by thermal fluctuations of any intensity). In spite of this different behavior at large γ , mobility in the optimal damping window (γ_m, γ_M) gets monotonically enhanced with decreasing T , no matter what the magnitude of A [panel(a)].

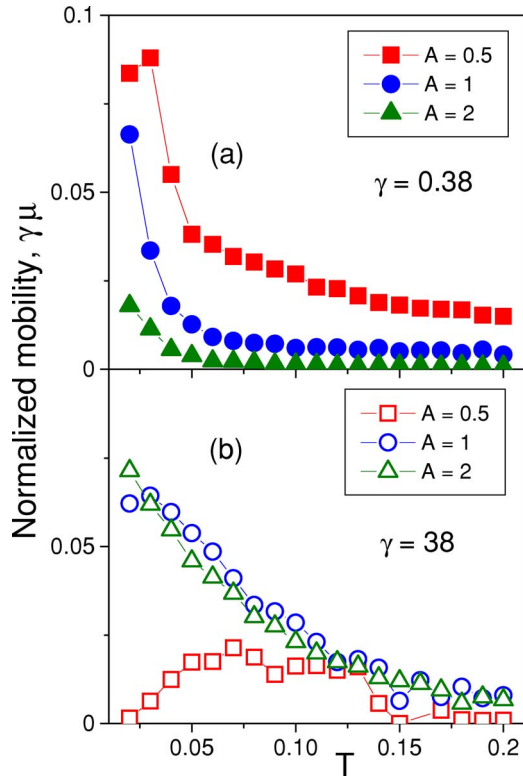


FIG. 5. (Color online) Temperature dependence of $\gamma\mu$ for different drive amplitudes A and two damping regimes: underdamped $\gamma=0.1\omega_0$ (open dots) and overdamped $\gamma=10\omega_0$ (solid dots). The ratchet dynamics (1) has been simulated for the harmonic potential (5) with $L=1$ and up-down ramp (4) with $\Omega=10^{-3}$.

Finally, we verified that the occurrence of an optimal rectification window is a robust property of underdamped ratchets. Following the prescriptions of Machura *et al.* [21], we checked that the enhanced ratchet mobility in the damping interval (γ_m, γ_M) corresponds to a strong suppression in its current fluctuations. Indeed, when operating a noise rectifier, one wants that its net current does not become swamped with the unavoidable fluctuations induced by the noise itself [22]. For instance, in Fig. 6 we compared the γ dependence of $\gamma\mu$ and of the dimensionless ratio

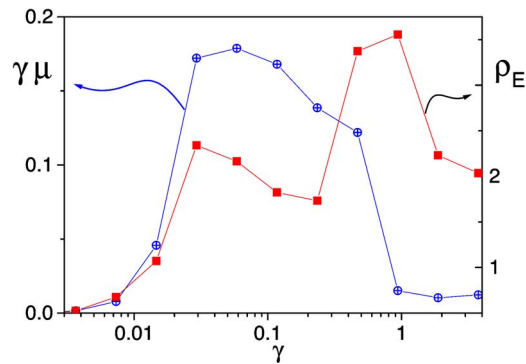


FIG. 6. (Color online) Curves $\gamma\mu$ and ρ_E vs γ for the inertial ratchet (1) with drive (3) and harmonic potential (5). Other simulation parameters are: $kT=0.03$, $A=0.5$, $L=1$, and $\Omega=10^{-3}$.

$$\rho_E = \frac{\langle v^4 \rangle - \langle v^2 \rangle^2}{\langle v^2 \rangle^2} \quad (14)$$

for the system (1) with $A < F_{3R}$. The quantity ρ_E represents the relative fluctuation intensity of the particle kinetic energy in the ratchet [21]. The rectification thresholds γ_m, γ_M are signaled by a surge in ρ_E , while inside the rectification window, fluctuations of the kinetic energy are drastically quenched. This result was to be expected in view of the analysis presented in Ref. [21].

V. CONCLUSIONS

In this work we have shown how operating a ratchetlike device under apparently similar conditions, namely, in the absence of noise (noiseless device, $T=0$) or at vanishingly low noise level ($T=0+$), leads to totally different rectification currents: chaotic and unpredictable in the former regime (also called deterministic), stable and strong within an optimal damping window in the latter one. These conclusions indicate inertia ratchets as a viable option to rectification in nanotechnology, as they can perform more efficiently than the more popular overdamped Brownian motors originally inspired by cellular biology.

Among the most promising implementations of a ratchet device are those aimed at rectifying the motion of the Josephson phase in SQUIDs [14] or vortices in superconductors [23], long Josephson junctions [12], and Josephson junction arrays [11]. Experimental testing is presently under way. In particular, recent experiments suggest that inertia is capable of enhancing the rectification current of vortices in superconducting films with periodic asymmetric pinning [24] or fluxons in current-biased annular Josephson junctions [25]. The advantages of Josephson-junction-based ratchets are nicely summarized in Ref. [12,14,25]: first, directed motion results in a net dc voltage, which is easy to measure; second, Josephson junctions are very fast devices that can operate (capture and rectify noise) in a broad frequency range from dc up to 100 GHz; and, most remarkably, third, by varying junction design and bath temperature, both overdamped and underdamped regimes are accessible. This last property, combined with the fact that the noise acting on such movable objects is very weak, makes our analysis particularly useful to determine the optimal operating conditions of a vortex ratchet device. It is important to emphasize that the rectification power of the Josephson junctions (see, e.g., Ref. [26]) is often very weak. Using underdamped Josephson junctions provide a way to remarkably boost the performance of Josephson-junction-based ratchets.

ACKNOWLEDGMENTS

This work was supported, in part, by the National Security Agency (NSA) and Advanced Research and Development Activity (ARDA) under Air Force Office of Research (AFOSR) Contract No. F49620-02-1-0334; and also supported by the US National Science Foundation Grant No. EIA-0130383.

- [1] P. Reimann, Phys. Rep. **361**, 57 (2002); P. Hänggi, F. Marchesoni, and F. Nori, Ann. Phys. **14**, 51 (2005).
- [2] R. Bartussek, P. Hänggi, and J. G. Kissner, Europhys. Lett. **28**, 459 (1994); R. D. Astumian and M. Bier, Phys. Rev. Lett. **72**, 1766 (1994).
- [3] J. Luczka, R. Bartussek, and P. Hänggi, Europhys. Lett. **31**, 431 (1995).
- [4] F. Marchesoni, Phys. Lett. A **237**, 126 (1998); B. Lindner, L. Schimansky-Geier, P. Reimann, P. Hanggi, and M. Nagaoka, Phys. Rev. E **59**, 1417 (1999).
- [5] P. Jung, J. G. Kissner, and P. Hänggi, Phys. Rev. Lett. **76**, 3436 (1996).
- [6] J. L. Mateos, Phys. Rev. Lett. **84**, 258 (2000); M. Barbi and M. Salerno, Phys. Rev. E **63**, 066212 (2001); H. A. Larrondo, C. M. Arizmendi, and F. Family, Physica A **320**, 119 (2003).
- [7] M. Borromeo, G. Costantini, and F. Marchesoni, Phys. Rev. E **65**, 041110 (2002).
- [8] B. A. Huberman, J. P. Crutchfield, and N. H. Packard, Appl. Phys. Lett. **37**, 750 (1980).
- [9] M. Schell, S. Fraser, and R. Kapral, Phys. Rev. A **26**, 504 (1982); S. Grossmann and H. Fujisaka, *ibid.* **26**, 1779 (1982); T. Geisel and J. Nierwetberg, Phys. Rev. Lett. **48**, 7 (1982).
- [10] For a review, see G. L. Baker and J. P. Gollub, *Chaotic Dynamics* (Cambridge University Press, Cambridge, England, 1990).
- [11] F. Faló, P. J. Martínez, J. J. Mazo, and S. Cilla, Europhys. Lett. **45**, 700 (1999).
- [12] E. Goldobin, A. Sterck, and D. Koelle, Phys. Rev. E **63**, 031111 (2001).
- [13] I. Zapata, R. Bartussek, F. Sols, and P. Hänggi, Phys. Rev. Lett. **77**, 2292 (1996).
- [14] A. Sterck, S. Weiss, and D. Koelle, Appl. Phys. A: Mater. Sci. Process. **A75**, 253 (2002); S. Weiss, D. Koelle, J. Müller, R. Gross, and K. Barthel, Europhys. Lett. **51**, 499 (2000).
- [15] For reviews, see the special issue in Appl. Phys. A: Solids Surf. 75 (2002) on *Ratchets and Brownian Motors: Basics, Experiments and Applications*, edited by H. Linke; and the issue in Chem. Phys. 281 (2002) on *Transport in Molecular Wires*, edited by P. Hänggi, M. Ratner, and S. Yaliraki.
- [16] H. Risken, *The Fokker-Planck Equation* (Springer, New York, 1984), Chap. 11.
- [17] F. Marchesoni, Phys. Lett. A **119**, 221 (1986).
- [18] S. Savel'ev, F. Marchesoni, P. Hänggi, and F. Nori, Europhys. Lett. **67**, 179 (2004); Phys. Rev. E **70**, 066109 (2004); Eur. Phys. J. B **40**, 403 (2004).
- [19] M. Borromeo, G. Costantini, and F. Marchesoni, Phys. Rev. Lett. **82**, 2820 (1999); M. Borromeo and F. Marchesoni, Phys. Lett. A **249**, 199 (1998).
- [20] V. I. Melnikov, Phys. Rep. **209**, 1 (1991).
- [21] L. Machura, M. Kostur, P. Talkner, J. Luczka, F. Marchesoni, and P. Hänggi, Phys. Rev. E **70**, 061105 (2004).
- [22] C. Costantini and F. Marchesoni, Europhys. Lett. **48**, 491 (1999); F. Marchesoni, Phys. Lett. A **231**, 61 (1997).
- [23] F. Marchesoni, Phys. Rev. Lett. **77**, 2364 (1996); J. F. Wambaugh, C. Reichhardt, C. J. Olson, F. Marchesoni, and F. Nori, *ibid.* **83**, 5106 (1999); C. S. Lee, B. Jankó, I. Derényi, and A. L. Barabási, Nature (London) **400**, 337 (1999); B. Y. Zhu, F. Marchesoni, and F. Nori, Phys. Rev. Lett. **92**, 180602 (2004).
- [24] J. Van de Vondel, C. C. de Souza Silva, B. Y. Zhu, M. Morelle, and V. V. Moshchalkov, Phys. Rev. Lett. **94**, 057003 (2005); S. Savelev, V. Misko, F. Marchesoni, and F. Nori, Phys. Rev. B **71**, 214303 (2005).
- [25] M. Beck, E. Goldobin, M. Neuhaus, M. Siegel, R. Kleiner, and D. Koelle, Phys. Rev. Lett. **95**, 090603 (2005).
- [26] J. B. Majer, J. Peguiron, M. Grifoni, M. Tusveld, and J. E. Mooij, Phys. Rev. Lett. **90**, 056802 (2003).